ACS APPLIED NANO MATERIALS

www.acsanm.org Article

Preparation Of Protein-Encapsulated Nanoparticles Using Polysuccinimide-Oleylamine For Sustained Protein Release

Xiangxun Chen, Cuong Hung Luu, Haotian Cha, Shehzahdi S. Moonshi, Jun Zhang, Nam-Trung Nguyen, and Hang Thu Ta*

Cite This: *ACS Appl. Nano Mater.* 2025, 8, 19658−19667 Read Online

ACCESS | Metrics & More | Article Recommendations

ABSTRACT: The clinical use of biologics for acute disease management is constrained by rapid clearance and systemic accumulation, which may compromise therapeutic outcomes. While sustained release nanoparticles are well-established for chronic conditions, analogous strategies for acute indications—particularly those requiring controlled release within 48 h—remain insufficiently developed. This study explores polysuccinimide-oleylamine (PSI-OA), a polymer with a tunable dissolution profile, for protein delivery. Using inverse flash nanoprecipitation and a herringbone T-shaped microfluidic mixer, PSI-OA nanoparticles encapsulating bovine serum albumin and lipase were fabricated. Optimized synthesis parameters yielded nanoparticles with less than 200 nm, with encapsulation efficiencies of roughly 75 and 98%, respectively, while retaining enzymatic activity. Both systems demonstrated ∼50% release at 24 h and full release by 48 h. These findings underscore the potential of PSI-OA nanoparticles for short-term sustained delivery of protein therapeutics in acute care settings.

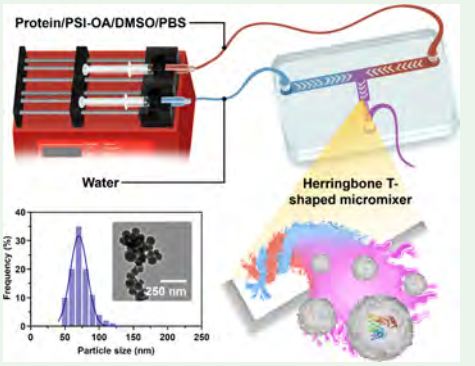

KEYWORDS: *flash nanoprecipitation, polysuccinimide, protein loading, sustained release, microfluidic, T-shaped mixer, herringbone*

1. INTRODUCTION

Extensive research on small-molecule drugs, known for their low molecular weight and ability to easily penetrate cell membranes, has yielded a vast arsenal of clinical therapeutic options.[1] However, their off-target effects and associated toxicities have prompted the exploration of alternative therapeutic strategies.[2] Thus, biological drugs (BDs) such as therapeutic protein have been gaining significance in the pharmaceutical market and clinical applications due to their greater precision and fewer adverse effects.[3] According to BBC Research, BDs contributed to a US$253 billion market share in 2020 and nearly doubled to US$452.9 billion in 2023. However, BDs often have a short half-life, necessitating frequent dosing to maintain therapeutic levels in the bloodstream. Frequent dosing can lead to wastage and harmful side effects.[4] Nanoparticles offer a promising strategy to overcome limitations associated with the short half-life and frequent dosing requirements of BDs.[4] Nanoparticles can be engineered to encapsulate BDs, protecting them from degradation and clearance in the body.[5] By improving drug stability, enabling targeted delivery, and facilitating controlled release, nanoparticles can enhance the specificity, efficiency, and overall therapeutic impact of BDs.[6] Nanoparticles have indeed been leveraged effectively for delivering BDs including RNA-based vaccines like those recently developed for severe acute respiratory syndrome coronavirus 2 (SARS-CoV-2).[7]

Existing materials, such as liposomal and inorganic nanoparticles, are limited by low loading capacity, loading efficiency, and potential toxicity.[8−10] Encapsulating BDs in a suitable polymeric carrier is a viable strategy to improve loading capacity and treatment efficacy. Various materials and nanoparticle synthesis methods for drug delivery have been investigated to date. For example, a study reported using poly(aspartic acid-*b*-lactic acid) to achieve a loading capacity of about 28%.[11] However, poly(lactic-*co*-glycolic acid) polymers often demonstrate slow degradation rates of over 7 days.[12,13] Conversely, a study using polyethylenimine-based nanoparticles to load insulin reported that 80% of the insulin was released within the first hour, which is unsuitable for therapeutic applications, which requires a delayed and gradual release over a period of 24−48 h or longer.[14] The main limitations of loading BDs in polymeric nanoparticles are low loading capacity, burst release of drugs, and restricted scalability. Conventional methods such as double emulsion are time-consuming and not suitable for large-scale produc-

Received: September 6, 2025
Revised: September 22, 2025
Accepted: September 24, 2025
Published: September 29, 2025

https://doi.org/10.1021/acsanm.5c04092
ACS Appl. Nano Mater. 2025, 8, 19658−19667

tion.[8] These challenges motivate the present study to assess novel polymeric materials for loading of BDs for the delayed and gradual release of various model proteins and enzymes in a 48 h period, providing guidance for future research applications.

Using conventional nanoprecipitation methods, we previously demonstrated the successful encapsulation of model proteins bovine serum albumin (BSA, 66 kDa) and lipase (LIP, 52 kDa) within polysuccinimide-oleylamine (PSI-OA) nanoparticles.[15] PSI-OA is a biodegradable and biocompatible polymer derived from aspartic acid[16−18] and has attracted recent interests as an efficient material for drug delivery.[19] This initial success motivated us to employ inverse flash nanoprecipitation, a common technique that utilizes solvents to induce phase separation for BD encapsulation in a micromixer. Current microreactors, such as a confined impinging jet (CIJ) mixer, which was inspired by the T mixer, facilitate faster nanoparticle nucleation and improve homogenization during the mixing process.[20] To date, the potential of PSI-OA to load BDs via CIJ still remains obscure. In our study, we developed a herringbone T-shaped (HTS) mixer to synthesize BSA or LIP-loaded PSI-OA nanoparticles and assessed its gradual release profile within a 48 h period. Herringbone structures are easy to fabricate compared to a more complicated CIJ mixer, which generates two counter-rotating vortices along the channel length.[20] A complete mixing cycle was achieved via the herringbone structure, leading to substantially enhanced mixing efficiency even at much lower flow rates.[21] The device comprises two inlets and one outlet, with the inlets positioned at the termini of the horizontal segment and the outlet located at the end of the vertical segment (Schemes 1 and 2). The T-shape of this microfluidic device allows two high-velocity solutions to converge at a junction and change direction, resulting in rapid mixing and synthesis. The following study evaluates key characteristics of the generated nanoparticles, including size distribution, polydispersity index (PDI), morphology, encapsulation efficiency, loading capacity, hydrolysis, release profiles, cytotoxicity, and enzyme activity of the loaded protein/enzymes.

Scheme 1. Schematic Representation of the Experimental Configuration for Synthesizing Protein- or Enzyme-Loaded PSI-OA Nanoparticles Using an HTS Mixer[a]

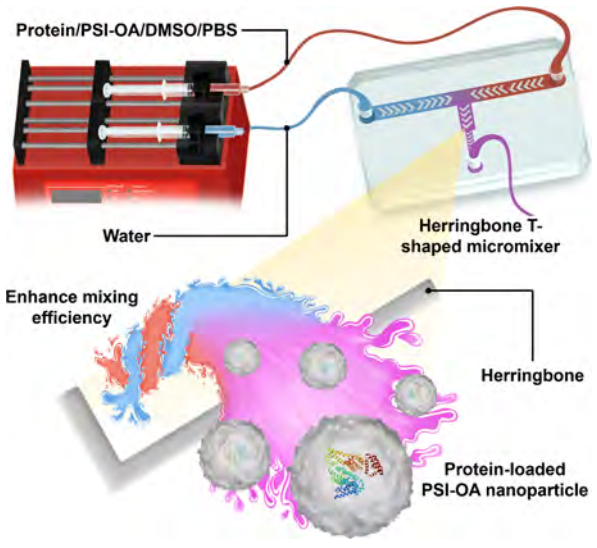

[a]A dual-syringe pump was employed to deliver two liquid streams at identical flow rates, with one inlet introducing a mixture of BSA and PSI-OA dissolved in a 1:1 v/v blend of PBS and DMSO, while the other inlet was perfused with DIW to induce rapid mixing, resulting in inverse flash precipitation and encapsulation to form the nanoparticles.

2. MATERIALS AND METHODS

2.1. Materials. L-Aspartic acid (≥98%), phosphoric acid (≥85 wt % in H_2O), sulfolane (99%), and oleylamine (OA, ≥98%) were obtained from Sigma-Aldrich (Missouri, United States). Bovine serum albumin (BSA) was acquired from Bovogen Biologicals Pty Ltd. (Victoria, Australia), while triacylglycerol acylhydrolase or lipase (LIP) was procured from ChemSupply Australia Pty Ltd. (South Australia, Australia). *N*,*N*-Dimethylformamide (DMF, 99%) and dimethyl sulfoxide (DMSO, 99.9%) were purchased from Thermo Fisher Scientific, Inc. (Massachusetts, United States). All other chemicals used in this study were sourced from commercial suppliers at analytical grade and utilized without any further purification.

2.2. Characterization Methods. *2.2.1. Hydrodynamic Properties.* The hydrodynamic diameter of nanoparticles suspended in solution was determined via dynamic light scattering (DLS, Anton Paar Litesizer 500, Anton Paar GmbH, Austria).

2.2.2. Microscopy. Transmission electron microscopy (TEM, JEOL JEM-1010, JEOL Ltd., Japan) was employed to visualize the size and morphology of the nanoparticles. The resultant TEM images served as the basis for particle size analysis, which was conducted using ImageJ software (National Institutes of Health, United States).

2.2.3. Spectroscopy. The absorbance or fluorescence intensity of the samples was measured utilizing a microplate reader (CLARIOstar Plus, BMG Labtech, Germany).

2.3. Synthesis of Polysuccinimide. Polysuccinimide (PSI) was synthesized via a polycondensation reaction of L-aspartic acid, following a method previously established and developed by our research group.[15,22] In a typical procedure, 21 g of an L-aspartic acid monomer was dissolved in 75 mL of sulfolane, with 1.5 mL of phosphoric acid added as a catalyst. The reaction was conducted in a 100 mL three-neck round-bottom flask, which was submerged in an oil bath maintained at 185 °C and purged with nitrogen gas. The mixture was stirred at 150 rpm using an overhead mechanical stirrer. After 6 h of reaction, the solution was allowed to cool and subsequently precipitated in 5 L of deionized water (DIW). The resulting PSI precipitate was washed three times with DIW to eliminate any residual solvent and unreacted reagents. The purified PSI was then dried in a vacuum oven at 60 °C until it was fully desiccated, after which the resulting powder was stored at ambient temperature.

2.4. Synthesis of Polysuccinimide-Oleylamine. Polysuccinimide-oleylamine (PSI-OA) was synthesized following a well-established protocol previously developed by our group.[15,22] Specifically, 10 mL of a PSI solution (100 mg mL^{-1} in DMF) was stirred at 500 rpm with 995 μL of OA at 70 °C for 12 h. Upon cooling to room temperature, the resulting product was subjected to three methanol washes—using a procedure analogous to that employed for PSI purification—in order to eliminate residual DMF. The purified polymer was subsequently dried under vacuum and stored at ambient conditions.

2.5. Fabrication of the Herringbone T-Shaped Micromixer. The microfluidic device employed in this study drew inspiration from the design principles of the confined impinging jet mixer, specifically to enhance mixing efficiency. In detail, the herringbone T-shaped (HTS) micromixer comprised two inlets and a single outlet; the inlets were situated at either end of the horizontal channel, while the outlet was positioned at the terminus of the vertical segment (see Schemes 1 and 2). In this research, we integrated herringbone structures along the channel to induce additional vortices, thereby facilitating improved mixing. Fabrication of the microfluidic chip was achieved through laser engraving, utilizing a CO_2 laser cutting machine (Rayjet 300, Trotec Laser GmbH, Austria) on a poly(methyl methacrylate)

https://doi.org/10.1021/acsanm.5c04092
ACS Appl. Nano Mater. 2025, 8, 19658−19667

Scheme 2. Schematic Design Illustrating the Detailed Dimensions of Components within the Herringbone T-Shaped Micromixer

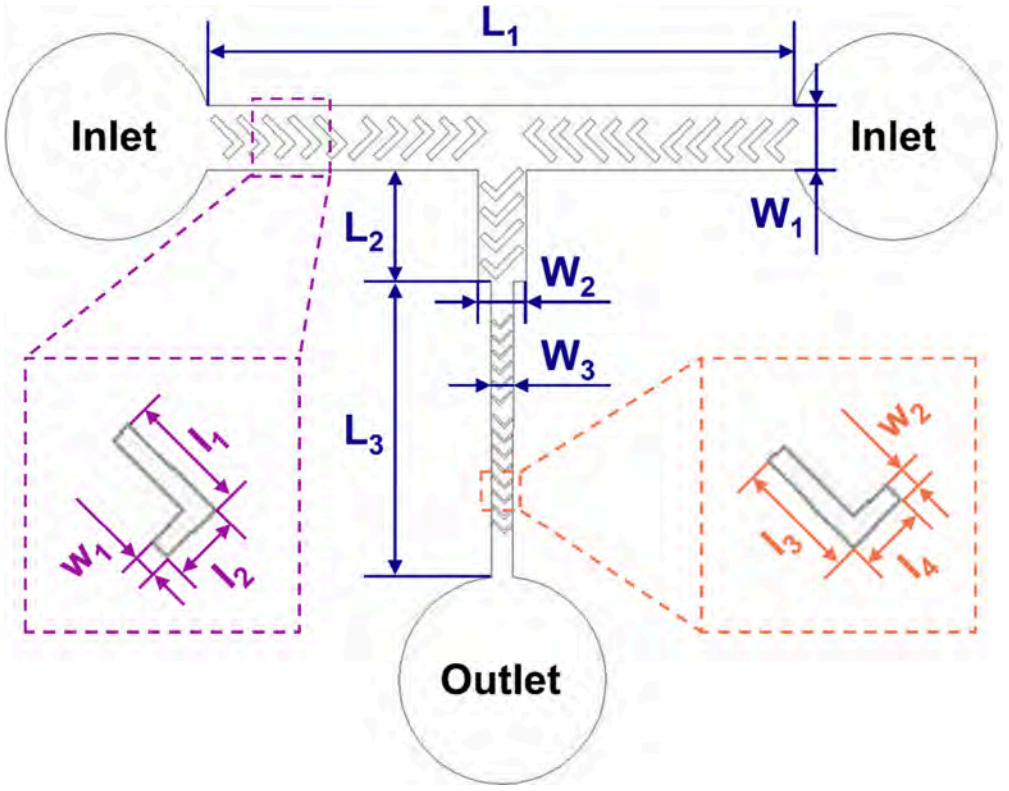

(PMMA) substrate. The dimensional parameters were denoted as L/l for length, W/w for width, and H for height. Specifically, the horizontal segment measured W_1 = 1.75 mm and L_1 = 16 mm. The vertical segment consisted of a dilated region (W_2 = 1.3 mm, L_2 = 3 mm) and a constricted region (W_3 = 0.5 mm, L_3 = 8 mm), with the overall channel height maintained at H_1 = 1.8 mm. Within each segment, staggered herringbone motifs were incorporated and aligned with the direction of flow. In the dilated sections of both regions, the herringbone structures were distributed, possessing L-shape dimensions of l_1 = 1 mm, l_2 = 0.6 mm, and w_1 = 0.2 mm. For the constricted sections, the herringbone measured l_3 = 0.5 mm, l_4 = 0.3 mm, and w_2 = 0.1 mm. The interherringbone gap in all segments was consistently maintained at approximately 0.4 mm. The height (H_2) of the herringbone features, measured from the base of the channel, was 0.9 mm.

The PMMA microfluidic device was fabricated by thermally bonding two layers of PMMA sheets using a heated platen (Specac Atlas GS15515, Specac Ltd., United Kingdom). One sheet was engraved with the desired channel pattern, while the other remained plain but was drilled with two inlets and a single outlet. Following laser cutting and engraving, both PMMA sheets were meticulously cleaned with isopropyl alcohol and aligned to ensure accurate registration of the microstructures. The assembly was subsequently placed in a hot embossing apparatus at 120 °C under a pressure of 12.5 bar for 20 min. The temperature was then lowered and maintained at 80 °C for a further 20 min to enhance the integrity of the bond. The device was finally cooled gradually under sustained pressure to prevent deformation and to consolidate the bond. This approach yielded a robust and homogeneous seal between the PMMA layers, thereby enabling the device to operate reliably under elevated flow rates and pressure conditions.

2.6. Synthesis of Protein-Loaded Nanoparticles. The synthesis of nanoparticles followed a protocol adapted with minor modifications from established methods.[15,23,24] Initially, a mixture comprising 0.2 mL of protein or enzyme solution in PBS and 0.2 mL of PSI-OA solution in DMSO was prepared. Subsequently, 0.4 mL of this mixture was transferred into a 1 mL syringe and connected to one inlet of the HTS mixer, while an equal volume (0.4 mL) of the nonsolvent DIW was similarly prepared and delivered to the other inlet. Both syringes were mounted onto a dual-syringe pump (SHENCHEN ISPLab02, Baoding Chuangrui Precision Pump Co., Ltd., China) to facilitate controlled mixing. The resulting nanoparticles were collected in 20 mL scintillation vials containing 3.2 mL of DIW under vigorous stirring at 1200 rpm for 5 min. PSI-OA concentrations were investigated in the range of 20−50 mg mL^{-1}, while BSA, employed as a model protein in this study, was evaluated for encapsulation at concentrations from 5 to 15 mg mL^{-1} and denoted as PSI-OA/BSA. Subsequently, LIP was encapsulated using the same methodology, based on the optimized parameters established for BSA, and the resulting formulation was denoted as PSI-OA/LIP. The synthesized product was subsequently subjected to centrifugation at 16,000g, after which the resulting pellet was redispersed in DIW.

2.7. Encapsulation Efficiency and Loading Capacity. The encapsulation efficiency (EE) and loading capacity (LC) of PSI-OA as a protein carrier were assessed by indirectly quantifying the unencapsulated protein/enzyme using a microBCA protein assay kit (Thermo Fisher Scientific, Inc., Massachusetts, United States). Specifically, 1.5 mL of the nanoparticle suspension was subjected to centrifugation at 16,000g for 15 min. The supernatant was subsequently collected to quantify the protein/enzyme content. The concentration of loaded protein in each experimental group was then determined based on a standard calibration curve generated using the same kit. The protocol for protein quantification was described in detail by the manufacturer. Both EE and LC values were calculated according to eqs 1 and 2 presented below.

$$\text{EE}\ (\%) = \frac{\text{weight of loaded protein}}{\text{weight of feeding protein}} \times 100\% \quad (1)$$

$$\text{LC}\ (\%) = \frac{\text{weight of loaded protein}}{\text{weight of nanoparticles and protein}} \times 100\% \quad (2)$$

https://doi.org/10.1021/acsanm.5c04092
ACS Appl. Nano Mater. 2025, 8, 19658−19667

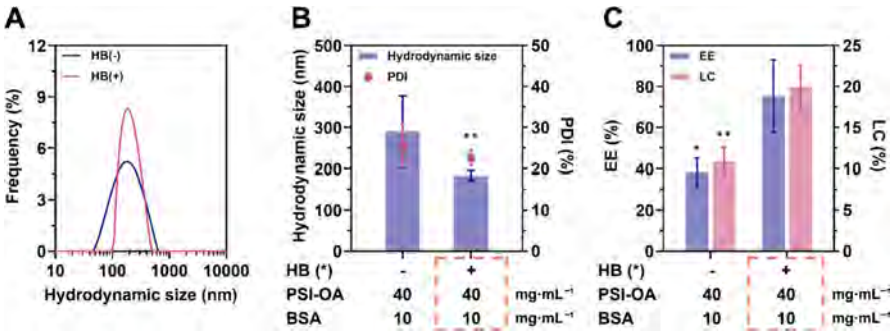

Figure 1. Impact of the herringbone structure and flow rate. (A) Intensity-weighted distribution, (B) hydrodynamic size and PDI, and (C) EE and LC of PSI-OA/BSA nanoparticles prepared using mixers with and without herringbone. The BSA:PSI-OA volume ratio was 1:1, and the flow rate was 20 mL min^{-1}. (*) HB denotes the herringbone structure, and boxed areas (orange) indicate optimal conditions. Statistical comparisons between experimental setups were performed using *t* tests.

2.8. Dissolution Study. Following synthesis, the nanoparticles were harvested and washed with DIW by means of centrifugation. This procedure was repeated three times to ensure thorough purification, after which the nanoparticles were redispersed in PBS at a concentration of 10 mg mL^{-1}. The resulting suspension was subsequently transferred into a 96-well plate and incubated at 37 °C in order to simulate *in vivo* physiological conditions. The absorbance at 320 nm was measured at specified intervals over a period of 48 h using a microplate reader.

2.9. *In Vitro* Release Study. The drug-loaded nanoparticles were suspended in phosphate-buffered saline (PBS) and incubated at 37 °C for 48 h. At designated intervals, 150 μL of the supernatant was withdrawn for protein quantification, and an equivalent volume of fresh PBS was added to restore the initial volume. The nanoparticles were pelleted by centrifugation at 16,000*g* for 15 min. The supernatant from each centrifuged sample was collected for concentration analysis. A Micro BCA protein assay kit was utilized to quantify the amounts of BSA and LIP released into the medium, following the manufacturer's protocol. These data were subsequently used to construct the cumulative release profile.

2.10. Cell Culture. *2.10.1. Cell Culture.* Chinese hamster ovary (CHO, ATCC CCL-61) cells were maintained in low-glucose Dulbecco's modified Eagle's medium (DMEM). The culture medium was further supplemented with 10% fetal bovine serum and 1% penicillin/streptomycin, thereby supporting robust cellular proliferation. All cultures were incubated under humidified conditions at 37 °C, with a 5% CO_2 atmosphere, to sustain optimal *in vitro* growth. Cells were routinely passaged or seeded for experimental procedures once they had reached approximately 90% confluency.

2.10.2. Cell Viability. In brief, CHO cells were seeded in 96-well plates at a density of 5×10^3 cells per 100 μL of culture medium per well and allowed to adhere overnight under standard conditions. The following day, the medium was aspirated and replaced with fresh medium containing BSA- or LIP-loaded PSI-OA nanoparticles at concentrations ranging from 0 to 1000 μg mL^{-1}, and the cells were incubated for either 24 or 48 h. Subsequently, the medium was removed and replaced with 100 μL of a PrestoBlue viability reagent (Thermo Fisher Scientific, Inc., Massachusetts, United States) diluted 1:10 in PBS, followed by a 30 min incubation. Viable cells were quantified by measuring fluorescence intensity at 560/590 nm (excitation/emission) using a microplate reader (CLARIOstar Plus-BMG Labtech). The fluorescence intensity obtained from untreated cells was set as the control, representing 100% cell viability.

2.11. Lipase Activity Assay. LIP activity was assessed using 4-nitrophenyl palmitate (NPP) as the substrate, with the procedure adapted from our previous work.[15] In detail, a volume of 50 μL substrate solution was prepared by dissolving 5 μL of 3 mg mL^{-1} NPP in isopropanol, combined with 44.8 μL of 50 mM Tris-HCl buffer and 0.2 μL of Triton X-100. To this mixture, 1.5 mL of PBS containing the released nanoparticles and LIP was added, and the reaction mixture was incubated at 37 °C for 60 min to allow for enzymatic activity. The reaction was terminated by placing the tubes on ice for 10 min. Subsequently, the resulting solution was transferred to a 96-well plate, and absorbance was measured at 400 nm using a microplate reader. A freshly prepared LIP solution in PBS was employed as a positive control throughout the study.

2.12. Statistical Analysis. All experiments were conducted in triplicate or greater. The results presented throughout this study are reported as means ± standard deviation. Graphical representations of the data were constructed using GraphPad Prism software (GraphPad Software, Inc., California, United States). Statistical significance was determined according to *p*-values, with $p \geq 0.05$ considered not significant (ns), $p < 0.05$ denoted as (*), $p < 0.01$ as (**), $p < 0.001$ as (***), and $p < 0.0001$ as (****).

3. RESULTS AND DISCUSSION

3.1. Impact of Herringbone Design. To begin with, the effectiveness of the herringbone architecture was assessed by comparing the efficiency of synthesizing protein-loaded nanoparticles using T-shaped micromixers with and without the herringbone design, as illustrated in Figure 1A–C. Specifically, Figure 1A shows that DLS analyses revealed no substantial difference in the mean particle sizes produced by either approach, with nanoparticles synthesized in the absence of the herringbone measuring 207.7 ± 112.7 nm, while those generated using the herringbone design exhibited a size of 219.1 ± 76.6 nm. Nonetheless, it was readily apparent that the particle size distribution was considerably more uniform when employing the HTS mixer. Upon encapsulation with BSA (Figure 1B), the nanoparticles synthesized without the herringbone achieved a size of 290.6 ± 87.4 nm and a PDI of 25.5 ± 5.5%. By contrast, those produced with the herringbone structure demonstrated improved uniformity and a reduced size, measuring 183.5 ± 12.4 nm and exhibiting a lower PDI of 22.6 ± 1.9. Furthermore, the EE and LC of PSI-OA/BSA nanoparticles fabricated with the herringbone structure were statistically superior, achieving 75.5 ± 17.6 and 20.0 ± 2.7%, respectively (Figure 1C).

These results collectively indicated that the incorporation of the herringbone structure substantially enhanced mixing efficiency, thereby promoting the effective formation of nanoparticles, reducing particle size and PDI, and improving protein loading. Such findings are consistent with prior reports, which demonstrated the advantages of the herringbone design for BD-loaded liposomal nanoparticles, chemically loaded nanoparticles, and gold-loaded polymeric nanoparticles.[25−28] Our present study therefore suggests that the application of herringbone structures warrants further exploration in the

https://doi.org/10.1021/acsanm.5c04092
ACS Appl. Nano Mater. 2025, 8, 19658−19667

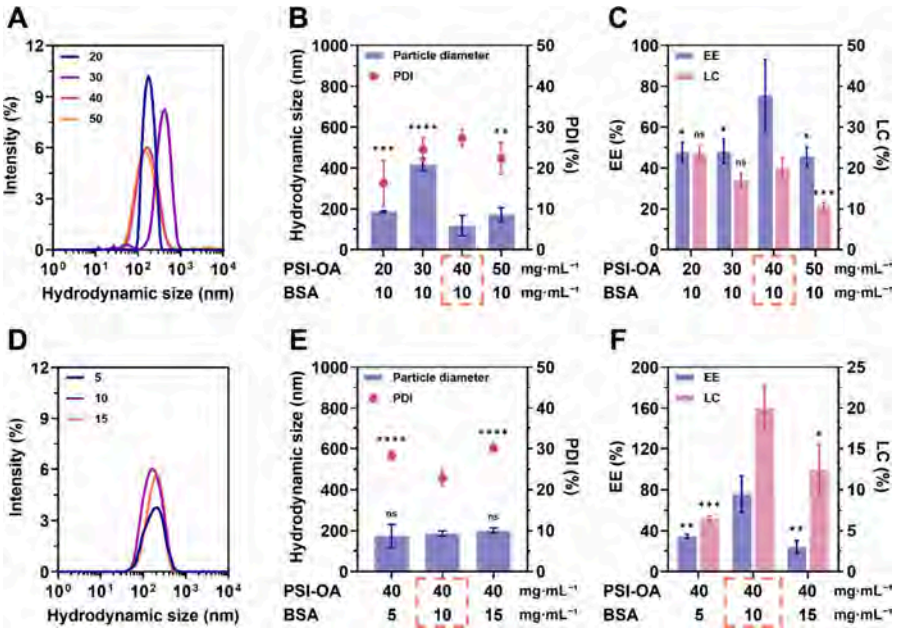

Figure 2. Optimization of PSI-OA/BSA nanoparticles by varying concentrations of PSI-OA and BSA. (A−C) Influence of PSI-OA concentration: (A) intensity-weighted particle size distribution, (B) mean hydrodynamic diameter and PDI, and (C) EE and LC of PSI-OA/BSA nanoparticles synthesized with different PSI-OA concentrations. (D−F) Influence of BSA concentration: (D) intensity-weighted particle size distribution, (E) mean hydrodynamic diameter and PDI, and (F) EE and LC of PSI-OA/BSA nanoparticles synthesized with varying BSA concentrations. Boxed regions (orange) indicate optimal formulation parameters. Statistical comparisons between the optimized group and all other groups were conducted using one-way ANOVA.

micromixer-assisted synthesis of BD-loaded polymeric nanoparticles.

3.2. Impact of PSI-OA and BSA Concentrations. Following the confirmation of the critical role of the herringbone structure in facilitating effective nanoprecipitation mixing with PSI-OA, we proceeded to adjust the component parameters in order to evaluate the influence of variables such as BSA and polymer concentration, while maintaining a constant flow rate of 20 mL min^{-1}, on the resultant physical attributes of the synthesized nanoparticles. As depicted in Figure 2A, increasing the PSI-OA concentration sequentially from 20 to 30, 40, and 50 mg mL^{-1} did not elicit a clear concentration-dependent variation in nanoparticle diameter. The intensity-weighted diameters were measured at 185.9 ± 46.4, 389.8 ± 116.5, 185.2 ± 12.7, and 179.1 ± 105.0 nm, respectively (Figure 2B).

A notable 2.2-fold increase in nanoparticle size, from 185.9 ± 46.4 to 389.8 ± 116.5 nm, was initially observed upon raising the PSI-OA concentration from 20 to 30 mg mL^{-1}. This size enlargement was likely attributed to an increase in the viscosity of the organic phase, which hindered solvent diffusion and consequently led to the formation of larger particles.[29,30] At a lower polymer concentration of 20 mg mL^{-1}, reduced nucleation efficiency may have resulted in the generation of smaller nanoparticles, whereas elevating the concentration to 30 mg mL^{-1} likely enhanced the nucleation process.[31] The EE values at 20 and 30 mg mL^{-1} were comparable, recorded at 47.8 ± 4.9 and 48.1 ± 6.0%, respectively; however, the LC dropped from 23.5 ± 1.8 to 17.0 ± 1.8%. Notably, the 40 mg mL^{-1} group yielded the smallest particle size among all groups, while also achieving the highest EE of 75.5 ± 17.6%. The LC, measured at 20.0 ± 2.7%, was statistically lower than that of the 20 mg mL^{-1} group but higher than that of the 50 mg mL^{-1} group, as illustrated in Figure 2C. It is possible that, at 50 mg mL^{-1}, the nucleation process had reached saturation, where PSI-OA exceeded its protein loading capacity, leading to the generation of surplus empty nanoparticles.[32] This hypothesis is supported by the marked decrease in EE (45.6 ± 4.8%) and LC (10.5 ± 1%) compared with the 20 mg mL^{-1} group. Additionally, a high PSI-OA concentration may have induced overly rapid nucleation, outpacing the diffusion of polymer chains to the growing nuclei. This phenomenon could have hindered the incorporation of the polymer into the nuclei, thereby limiting particle growth and mobility and yielding smaller particles. Agglomeration during this rapid nucleation might also have contributed to the formation of slightly larger particles compared with the 40 mg mL^{-1} group.[32,33] Consequently, a PSI-OA concentration of 40 mg mL^{-1} at a flow rate of 20 mL min^{-1} were selected for subsequent experiments.

Figure 2D−F illustrates the influence of varying BSA concentrations on the particle size and polydispersity of PSI-OA nanoparticles. At a BSA concentration of 5 mg mL^{-1}, the intensity-weighted diameter was 174.7 ± 56.0 nm. A moderate increase in BSA concentration to 10 mg mL^{-1} resulted in a marginal change in size, reaching 185.2 ± 12.7 nm. However, further elevating the BSA concentration to 15 mg mL^{-1} led to a more pronounced increase in particle size, measured at 200.5 ± 12.7 nm. Nanoparticles synthesized at the lowest BSA concentration (5 mg mL^{-1}) displayed greater variability, as evidenced by a significantly higher PDI (28.3 ± 1.1%) in comparison to the 10 mg mL^{-1} group (22.9 ± 1.93%). At 15 mg mL^{-1}, the particle size increased, and the PDI also rose markedly to 30.1 ± 1.0%, surpassing the threshold of 25% and suggesting a broader size distribution and less monodisperse formulation (Figure 2E). The EE for the 10 mg mL^{-1} BSA group reached 75.5 ± 17.6%, which was substantially higher than those of the 5 and 15 mg mL^{-1} groups, at 34.4 ± 2.0 and

https://doi.org/10.1021/acsanm.5c04092
ACS Appl. Nano Mater. 2025, 8, 19658−19667

26.1 ± 17.6%, respectively (Figure 2F). The LC also followed a similar trend, with the 10 mg mL^{-1} formulation achieving 20.0 ± 2.7%, compared to only 6.5 ± 0.4 and 12.4 ± 3.1% for the 5 and 15 mg mL^{-1} groups, respectively. The low EE and LC observed in the 15 mg mL^{-1} group may reflect the saturation point of PSI-OA's capacity to encapsulate BSA via the precipitation method, consistent with challenges reported for other polymeric nanoparticle systems involving variable drug loadings.[15,34] In conclusion, the optimal synthesis conditions using the HTS mixer were determined to be 40 mg mL^{-1} PSI-OA and 10 mg mL^{-1} BSA at a flow rate of 20 mL min^{-1}.

3.3. Characteristics of PSI-OA/BSA Nanoparticles. Under the optimized synthesis conditions, the resulting formulation yielded nanoparticles with an intensity-distributed diameter of 185.2 ± 12.7 nm and a zeta potential of −39.1 ± 1.1 mV. Moreover, the TEM image (Figure 3A) revealed that

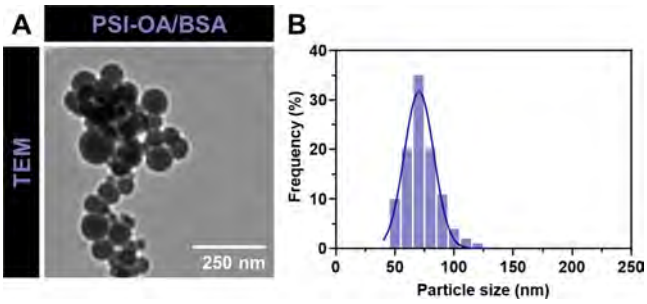

Figure 3. Morphological characteristics of PSI-OA/BSA nanoparticles. (A) TEM image and (B) particle size distribution of BSA-loaded PSI-OA nanoparticles.

the BSA-loaded nanoparticles synthesized under these parameters possessed a well-defined spherical morphology, with a particle size of 73.3 ± 7.7 nm as quantified via ImageJ (Figure 3B). Collectively, these outcomes reinforced the suitability of the HTS mixer for fabricating protein- or enzyme-encapsulated nanoparticles by significantly enhancing the mixing efficiency and promoting improved particle uniformity.

3.4. Characterization of PSI-OA/LIP Nanoparticles. For the PSI-OA/LIP nanoparticles, the synthesis conditions optimized for BSA were adopted, while the influence of the flow rate was re-evaluated. In theory, elevating the flow rate during nanoparticle formation is anticipated to reduce particle size and improve PDI.[35] In this study, at a flow rate of 75 mL min^{-1}, DLS analysis (Figure 4B) showed an intensity-distributed curve with a minor peak at 28.1 ± 3.4 nm and a major peak at 879.6 ± 125.8 nm. Overall, the intensity-weighted hydrodynamic diameter of nanoparticles synthesized under these conditions markedly exceeded the ideal size range suited for applications such as intravenous drug delivery.[36] Particles smaller than 200 nm are generally known to circulate more effectively than those exceeding 300 nm. The elevated PDI of 27.8% suggested substantial heterogeneity in particle dimensions. The TEM image presented in Figure 4A confirmed the presence of spherical particles with irregular and varied morphologies, consistent with the broad size distribution. In contrast, the PSI-OA/LIP nanoparticles synthesized under the optimized conditions exhibited an intensity-distributed diameter of 155.8 ± 29.8 nm, a PDI of 20.5 ± 6.8%, and a zeta potential of −41.7 ± 1.6 mV. The EE and LC reached 98.2 ± 0.3 and 23.3 ± 0.2%, respectively representing 1.3-fold and 1.15-fold increases compared to the BSA-loaded formulation. However, these differences were not statistically significant when compared across the two groups synthesized at different flow rates (Figure 4C).

Nonetheless, according to the TEM image (Figure 4A), the sample synthesized at a high flow rate adhered to the established principle that an increase in the flow rate is generally associated with a reduction in particle size.[35] The variability observed in the DLS data could plausibly be attributed to light scattering artifacts caused by a small proportion of large aggregates, which skewed the intensity-based average diameter toward the micrometer scale and consequently elevated the PDI. Although the intensity-weighted distribution appeared inconsistent, the number-weighted analysis exhibited a dominant peak at approximately 20 nm with a secondary peak around 15 nm, suggesting that the majority of the particles were indeed small. The disproportionate influence of a few larger species—possibly formed via aggregation or as oversized particles during synthesis—may explain the observed distortion in the intensity profile. Such aggregation phenomena are more frequently encountered with nonspherical morphologies but can also arise under the present conditions.[37,38] Furthermore, the zeta potential of the LIP-loaded nanoparticles prepared at the high flow rate was −30.3 ± 2.5 mV, noticeably more positive than the −41.7 ± 1.6 mV observed in the low-flow-rate group, which may have contributed to the marginal aggregation tendency.[39,40] Nevertheless, the successful synthesis of nanoparticles with diameters below 50 nm presents a significant advantage, as this size range facilitates translocation across vascular barriers with low permeability, including the blood–brain barrier. Nanoparticles of this scale have consistently demonstrated enhanced transport efficiency when compared with their larger counterparts.[41] Such characteristics hold considerable promise for future therapeutic strategies targeting acute conditions, notably ischemic stroke, as well as tumors exhibiting restricted vascular permeability, such as those of the brain and pancreas.[42] In conclusion, strategies to improve the stability of the nanoparticulate system should also be taken into account. These may include the modulation of zeta potential to enhance electrostatic repulsion among particles, or the incorporation of additional stabilizing agents within the formulation to prevent aggregation and maintain colloidal integrity.

3.5. Dissolution, Controlled Release, and Lipase Activity Studies. The dissolution behavior of the synthesized PSI-OA nanoparticles loaded with either BSA or LIP was systematically investigated. Specifically, the nanoparticles were suspended in PBS and incubated at 37 °C. Their dissolution was monitored via a reduction in absorbance measured at a wavelength of 320 nm, whereby a stable normalized absorbance value near 1 indicated colloidal stability over time. As illustrated in Figure 4D, the dissolution profile of BSA-loaded PSI-OA nanoparticles demonstrated a slow initial degradation over the first 3 h, followed by a pronounced lag phase of approximately 9 h, and thereafter, a continued decline until complete hydrolysis was achieved at 36 h. In contrast, PSI-OA/LIP nanoparticles exhibited no notable delay, undergoing a steady and uninterrupted dissolution process that culminated in complete degradation between 42 and 45 h.

Regarding the release profiles of both nanoparticle formulations, the BSA-loaded PSI-OA nanoparticles exhibited

https://doi.org/10.1021/acsanm.5c04092
ACS Appl. Nano Mater. 2025, 8, 19658−19667

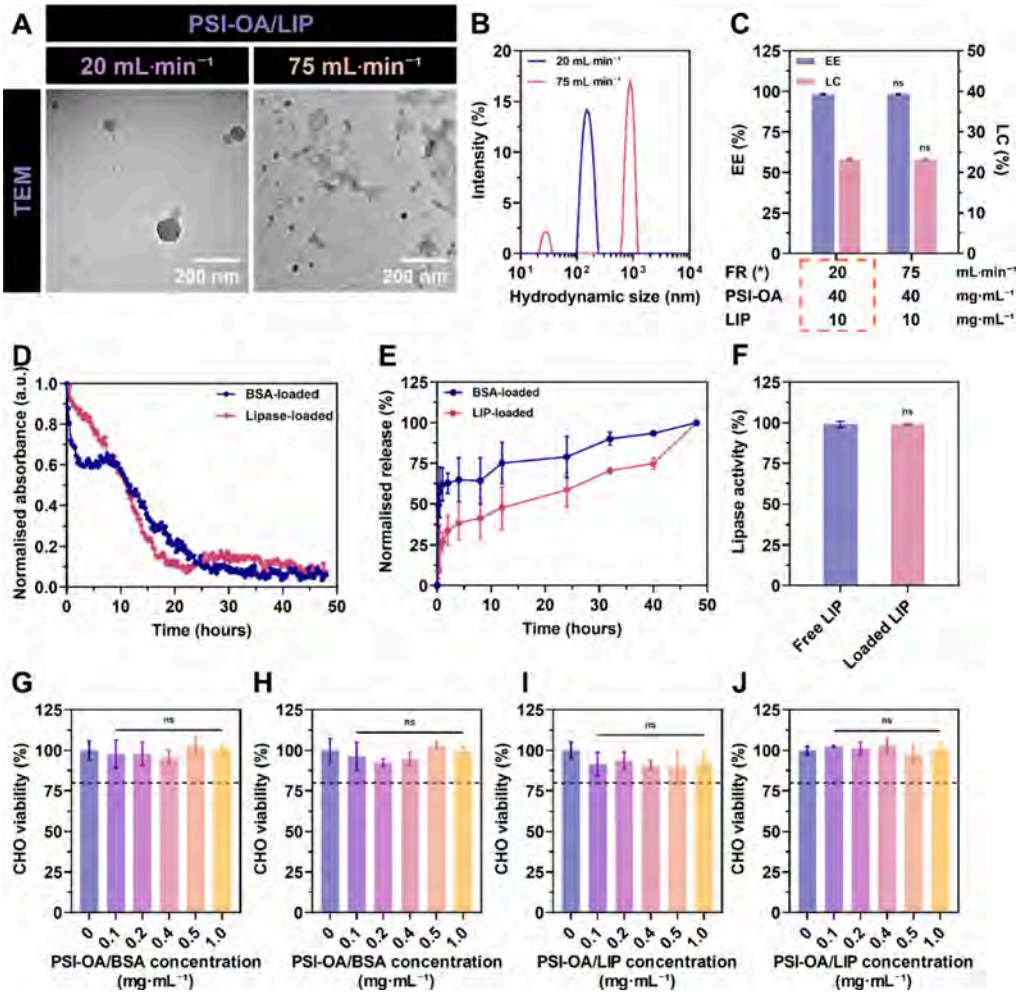

Figure 4. Characteristics of PSI-OA/LIP nanoparticles (A–C): (A) TEM images, (B) hydrodynamic size, and (C) EE and LC of PSI-OA/LIP nanoparticles synthesized at the flow rates of 20 and 75 mL min^{-1}. Characteristics of protein-loaded PSI-OA nanoparticles (D–F): (D) dissolution and (E) release profile of the nanoparticles. (F) Normalized LIP activity. Cytotoxicity studies of protein-loaded PSI-OA nanoparticles with CHO cells (G–J): cell viability of PSI-OA/BSA after (G) 24 and (H) 48 h. Cell viability of PSI-OA/LIP after (I) 24 and (J) 48 h. (*) FR refers to the applied flow rate; boxed areas (orange) indicate optimal conditions. Statistical comparisons between experimental setups were performed using *t* tests.

an initial burst release within the first 15 min, during which 49.4 ± 12.9% of the encapsulated BSA was released, as shown in Figure 4E. The cumulative release exceeded 60% after 3 h and subsequently reached 79.0 ± 12.8 and 90.1 ± 3.9% at the 24 and 32 h time points, respectively. This release behavior was consistent with the previously observed dissolution kinetics. By contrast, the LIP-loaded nanoparticles demonstrated a more restrained initial release, with 26.8 ± 6.0% of the payload released within the first hour. The release proceeded in a gradual manner, reaching 47.5 ± 12.8% at 12 h and achieving complete release by 48 h, thereby corroborating the dissolution profile of the PSI-OA/LIP formulation.

The release rates of BSA observed in this study were notably faster than those reported for PSI-OA nanoparticles previously synthesized using a conventional two-step nanoprecipitation approach.[15] Nevertheless, the LIP-loaded group maintained a comparatively slow-release behavior overall. This finding suggests that the degree of interaction and encapsulation between the PSI-OA carrier and different protein types varies. Specifically, LIP, an enzyme that hydrolyses lipids at hydrophobic interfaces, demonstrated a strong affinity for the OA core of the PSI-OA nanoparticles via hydrophobic interactions, thereby contributing to its sustained release profile. Additionally, it may be inferred that nanoparticles fabricated using the HTS mixer strategy exhibited a faster release due to a less densely packed internal structure, in contrast to nanoparticles prepared via alternative techniques such as flash nanoprecipitation, which have previously been employed to produce low-density particles for aerosol applications.[43] The reduced density likely facilitated the penetration of PBS into the polymeric matrix, thereby accelerating protein release.[44] It is worth noting that, owing to current technological constraints, the distinction between the encapsulated protein and the polymeric matrix within the nanoparticles remains difficult to resolve using conventional imaging methods such as TEM.[5]

The influence of PSI-OA and the HTS mixer on protein activity was evaluated by comparing freshly prepared LIP with PSI-OA/LIP nanoparticles. The enzymatic activity of LIP released from the nanoparticles was comparable to that of the fresh control (Figure 4F), indicating that the activity of the enzyme was retained following encapsulation within the PSI-OA matrix. These findings support earlier observations that

https://doi.org/10.1021/acsanm.5c04092
ACS Appl. Nano Mater. 2025, 8, 19658–19667

PSI-OA can preserve the functionality of proteins and enzymes, thereby validating its suitability as a carrier in therapeutic contexts. Moreover, this study provides a proof of concept for the preparation of BD-loaded PSI-OA nanoparticles via the inverse flash nanoprecipitation technique using the HTS mixer.

To evaluate the *in vitro* biocompatibility of the synthesized nanoparticles, CHO cells were exposed to increasing concentrations of PSI-OA/BSA and PSI-OA/LIP. Following 24 h of incubation, cell viability remained above 80% across all tested concentrations for both formulations (Figure 4G–J). Even after 48 h, when exposed to a nanoparticle concentration as high as 1 mg mL^{-1}, CHO cells maintained viability around 90–100%, indicating no observable cytotoxic effects. These results confirmed that both BSA- and LIP-loaded nanoparticles exhibited excellent cytocompatibility.

Altogether, this study demonstrates that PSI-OA, when formulated via HTS mixer-assisted synthesis, represents a viable carrier for protein encapsulation in biomedical applications. This system offers multiple benefits, such as rapid yet controlled release profiles that preserve bioactivity, reduce nonspecific accumulation, and ensure high biocompatibility, making it highly promising for precise therapeutic delivery.

4. CONCLUSIONS AND FUTURE PERSPECTIVES

Flash nanoprecipitation is a promising method for preparing surfactant- and stabilizer-free nanoparticles for protein encapsulation. Previous studies have explored this technique with various BDs and polymers.[20,45] In this work, we investigated the use of BSA and LIP-loaded PSI-OA nanoparticles for gradual release over 48 h. PSI is a precursor in the alkaline hydrolysis process that creates poly(aspartic acid) (PASP), a bioactive polypeptide. In milder conditions (neutral pH), PSI can hydrolyze to PASP, although the process is slower.[22,46] Because of this characteristic, PSI can be used to regulate BD loading and release. The PSI backbone was grafted with OA to control the hydrolysis and dissolution of PSI nanoparticles. To our best knowledge, this is the first study utilizing a herringbone T-shaped mixer to facilitate flash nanoprecipitation for BD-loaded nanoparticle synthesis. Our results showed that PSI-OA synthesized using this approach demonstrates distinct physical features including controllable size, gradual release of the BDs, and hydrolysis of the polymer over 48 h. The PSI-OA system demonstrated its capacity to preserve the enzymatic activity of LIP. Furthermore, the optimization process revealed that the interaction between PSI-OA and loaded proteins was protein-specific, indicating distinct behaviors depending on the nature of the biomacromolecule. Although the majority of parameters directly associated with the synthesis protocol were successfully optimized, further investigations are warranted to elucidate the underlying mechanisms governing BD loading, as well as to explore the potential of this system in biological and therapeutic applications. Overall, this study provides a valuable foundation for more targeted and application-specific research in the future.

■ ASSOCIATED CONTENT

Data Availability Statement

Data will be made available on request.

■ AUTHOR INFORMATION

Corresponding Author

Hang Thu Ta − *School of Environment and Science and Queensland Quantum and Advanced Technologies Research Institute, Griffith University, Nathan, QLD 4111, Australia;* orcid.org/0000-0003-1188-0472; Email: h.ta@griffith.edu.au

Authors

Xiangxun Chen − *School of Environment and Science and Queensland Quantum and Advanced Technologies Research Institute, Griffith University, Nathan, QLD 4111, Australia;* orcid.org/0000-0002-2208-1038

Cuong Hung Luu − *School of Environment and Science and Queensland Quantum and Advanced Technologies Research Institute, Griffith University, Nathan, QLD 4111, Australia;* orcid.org/0000-0002-0919-5911

Haotian Cha − *School of Environment and Science and Queensland Quantum and Advanced Technologies Research Institute, Griffith University, Nathan, QLD 4111, Australia*

Shehzahdi S. Moonshi − *School of Environment and Science and Queensland Quantum and Advanced Technologies Research Institute, Griffith University, Nathan, QLD 4111, Australia;* orcid.org/0000-0003-2048-595X

Jun Zhang − *Queensland Quantum and Advanced Technologies Research Institute, Griffith University, Nathan, QLD 4111, Australia;* orcid.org/0000-0003-1113-6264

Nam-Trung Nguyen − *Queensland Quantum and Advanced Technologies Research Institute, Griffith University, Nathan, QLD 4111, Australia*

Complete contact information is available at: https://pubs.acs.org/10.1021/acsanm.5c04092

Notes

The authors declare no competing financial interest.

■ ACKNOWLEDGMENTS

This study is funded by the National Health and Medical Research Council (H.T.T.: APP1182347 and APP2002827). X.C., C.L. and H.C. are supported by PhD scholarships from Griffith University. S.S.M. is supported by a Griffith University fellowship. N.-T.N. is supported by an Australian Research Council Laureate Fellowship (FL230100023). H.T.T. is supported by a Heart Foundation Future Leader Fellowship (102761) and an Australian Research Council Future Fellowship (FT240100280). This work was performed in part at the Queensland node of the Australian National Fabrication Facility established under the National Collaborative Research Infrastructure Strategy to provide nano- and microfabrication facilities for Australia's researchers.

■ REFERENCES

(1) Beck, H.; Härter, M.; Haß, B.; Schmeck, C.; Baerfacker, L. Small molecules and their impact in drug discovery: A perspective on the occasion of the 125th anniversary of the Bayer Chemical Research Laboratory. *Drug Discovery Today.* **2022**, *27* (6), 1560–1574.

(2) Zhao, Z.; Ukidve, A.; Kim, J.; Mitragotri, S. Targeting Strategies for Tissue-Specific Drug Delivery. *Cell* **2020**, *181* (1), 151–167.

(3) Kumar, V.; Barwal, A.; Sharma, N.; Mir, D. S.; Kumar, P.; Kumar, V. Therapeutic proteins: developments, progress, challenges, and future perspectives. *3 Biotech* **2024**, *14* (4), 112.

(4) Phan, V. H. G.; Nguyen, B.-P. T.; Nguyen, N. Y.; Tran, C.-N. D.; Nguyen, Q.-N. D.; Luu, C. H.; Manivasagan, P.; Jang, E.-S.; Yang, D.

C.; Yang, D. U.; Li, Y.; Conde, J.; Thambi, T. Longan-inspired chitosan-pectin core-shell hydrogel beads for oral delivery of biodrugs to enhance osteoporosis therapy. *Int. J. Biol. Macromol.* **2025**, *308*, No. 142254.
(5) Pagels, R. F.; Prud'homme, R. K. Polymeric nanoparticles and microparticles for the delivery of peptides, biologics, and soluble therapeutics. *J. Contr. Release* **2015**, *219*, 519−535.
(6) Mitchell, M. J.; Billingsley, M. M.; Haley, R. M.; Wechsler, M. E.; Peppas, N. A.; Langer, R. Engineering precision nanoparticles for drug delivery. *Nat. Rev. Drug Discovery* **2021**, *20* (2), 101−124.
(7) Thi, T. T. H.; Suys, E. J. A.; Lee, J. S.; Nguyen, D. H.; Park, K. D.; Truong, N. P. Lipid-Based Nanoparticles in the Clinic and Clinical Trials: From Cancer Nanomedicine to COVID-19 Vaccines. *Vaccines* **2021**, *9* (4), 359.
(8) Chen, X.; Wu, Y.; Dau, V. T.; Nguyen, N.-T.; Ta, H. T. Polymeric nanomaterial strategies to encapsulate and deliver biological drugs: points to consider between methods. *Biomater. Sci.* **2023**, *11* (6), 1923−1947.
(9) Luu, H.-C.; Ngo, C. Q.; Nguyen, N. H.; Tran, D. L.; Nguyen, D. H.; Nguyen, C. K. Polyamidoamine dendrite-tailored mesoporous nanosilica surfaces for high drug loading and controlled release. *VJSTE* **2023**, *65* (1), 25−31.
(10) Li, Y.; Giang Phan, V. H.; Pan, Z.; Xuan, X.; Yang, H. Y.; Luu, C. H.; Phan, T.-H.; Le, T. M. D.; Thambi, T. Integrated and hyaluronic acid-coated mesoporous silica nanoparticles conjugated with cisplatin and chlorin e6 for combined chemo and photodynamic cancer therapy. *Eur. Polym. J.* **2024**, *220*, No. 113426.
(11) Markwalter, C. E.; Pagels, R. F.; Hejazi, A. N.; Gordon, A. G. R.; Thompson, A. L.; Prud'homme, R. K. Polymeric Nanocarrier Formulations of Biologics Using Inverse Flash NanoPrecipitation. *AAPS Journal* **2020**, *22* (2), 18.
(12) Iyer, R.; Kuriakose, A. E.; Yaman, S.; Su, L. C.; Shan, D.; Yang, J.; Liao, J.; Tang, L.; Banerjee, S.; Xu, H.; Nguyen, K. T. Nanoparticle eluting-angioplasty balloons to treat cardiovascular diseases. *Int. J. Pharm.* **2019**, *554*, 212−223.
(13) Fredenberg, S.; Wahlgren, M.; Reslow, M.; Axelsson, A. The mechanisms of drug release in poly(lactic-co-glycolic acid)-based drug delivery systems—A review. *Int. J. Pharm.* **2011**, *415* (1), 34−52.
(14) Salvioni, L.; Fiandra, L.; Del Curto, M. D.; Mazzucchelli, S.; Allevi, R.; Truffi, M.; Sorrentino, L.; Santini, B.; Cerea, M.; Palugan, L.; Corsi, F.; Colombo, M. Oral delivery of insulin via polyethylene imine-based nanoparticles for colonic release allows glycemic control in diabetic rats. *Pharmacol. Res.* **2016**, *110*, 122−130.
(15) Chen, X.; Moonshi, S. S.; Nguyen, N.-T.; Ta, H. T. Preparation of protein-loaded nanoparticles based on poly(succinimide)-oleylamine for sustained protein release: a two-step nanoprecipitation method. *Nanotechnology* **2024**, *35* (5), No. 055101.
(16) Adelnia, H.; Tran, H.; Little, P.; Blakey, I.; Ta, H. Poly (aspartic acid) in biomedical applications: from polymerization, modification, properties, degradation, and biocompatibility to applications. *ACS Biomater. Sci. Eng.* **2021**, *7*, 2083−2105.
(17) Adelnia, H.; Sirous, F.; Blakey, I.; Ta, H. T. Metal ion chelation of poly (aspartic acid): From scale inhibition to therapeutic potentials. *Int. J. Biol. Macromol.* **2023**, *229*, 974−993.
(18) Adelnia, H.; Blakey, I.; Little, P. J.; Ta, H. T. Hydrogels based on poly (aspartic acid): synthesis and applications. *Front. Chem.* **2019**, *7*, 755.
(19) Moonshi, S. S.; Vazquez-Prada, K. X.; Adelnia, H.; van Holthe, N. J. W.; Wu, Y.; Tang, J.; Bulmer, A. C.; Ta, H. T. Polysuccinimide-based nanoparticle: A nanocarrier with drug release delay and zero burst release properties for effective theranostics of cancer. *Appl. Mater. Today* **2024**, *37*, No. 102150.
(20) Han, J.; Zhu, Z.; Qian, H.; Wohl, A. R.; Beaman, C. J.; Hoye, T. R.; Macosko, C. W. A simple confined impingement jets mixer for flash nanoprecipitation. *J. Pharm. Sci.* **2012**, *101* (10), 4018−4023.
(21) Williams, M. S.; Longmuir, K. J.; Yager, P. A practical guide to the staggered herringbone mixer. *Lab Chip* **2008**, *8* (7), 1121−1129.
(22) Adelnia, H.; Moonshi, S. S.; Wu, Y.; Bulmer, A. C.; McKinnon, R.; Fastier-Wooller, J. W.; Blakey, I.; Ta, H. T. A Bioactive Disintegrable Polymer Nanoparticle for Synergistic Vascular Anti-calcification. *ACS Nano* **2023**, *17* (19), 18775−18791.
(23) Feng, J.; Markwalter, C. E.; Tian, C.; Armstrong, M.; Prud'homme, R. K. Translational formulation of nanoparticle therapeutics from laboratory discovery to clinical scale. *J. Transl. Med.* **2019**, *17* (1), 200.
(24) Markwalter, C. E.; Prud'homme, R. K. Design of a Small-Scale Multi-Inlet Vortex Mixer for Scalable Nanoparticle Production and Application to the Encapsulation of Biologics by Inverse Flash NanoPrecipitation. *J. Pharm. Sci.* **2018**, *107* (9), 2465−2471.
(25) Rahali, K.; Tabriz, A. G.; Douroumis, D. The effect of 3D printed microfluidic array designs on the preparation of liposome nanoparticles. *J. Drug Delivery Sci. Technol.* **2024**, *94*, No. 105411.
(26) Li, Y.; Lee, R. J.; Huang, X.; Li, Y.; Lv, B.; Wang, T.; Qi, Y.; Hao, F.; Lu, J.; Meng, Q.; Teng, L.; Zhou, Y.; Xie, J.; Teng, L. Single-step microfluidic synthesis of transferrin-conjugated lipid nanoparticles for siRNA delivery. *Nanomedicine: Nanotechnol. Biol. Med.* **2017**, *13* (2), 371−381.
(27) Sun, Y.; Lee, R. J.; Meng, F.; Wang, G.; Zheng, X.; Dong, S.; Teng, L. Microfluidic self-assembly of high cabazitaxel loading albumin nanoparticles. *Nanoscale* **2020**, *12* (32), 16928−16933.
(28) Cheheltani, R.; Ezzibdeh, R. M.; Chhour, P.; Pulaparthi, K.; Kim, J.; Jurcova, M.; Hsu, J. C.; Blundell, C.; Litt, H. I.; Ferrari, V. A.; Allcock, H. R.; Sehgal, C. M.; Cormode, D. P. Tunable, biodegradable gold nanoparticles as contrast agents for computed tomography and photoacoustic imaging. *Biomaterials* **2016**, *102*, 87−97.
(29) Guhagarkar, S. A.; Malshe, V. C.; Devarajan, P. V. Nanoparticles of polyethylene sebacate: a new biodegradable polymer. *AAPS PharmSciTech* **2009**, *10* (3), 935−942.
(30) Sharma, N.; Madan, P.; Lin, S. Effect of process and formulation variables on the preparation of parenteral paclitaxel-loaded biodegradable polymeric nanoparticles: A co-surfactant study. *Asian J. Pharm. Sci.* **2016**, *11* (3), 404−416.
(31) Meldrum, F. C.; Colfen, H. Crystallization and formation mechanisms of nanostructures. *Nanoscale* **2010**, *2* (11), 2326−2327.
(32) Thanh, N. T. K.; Maclean, N.; Mahiddine, S. Mechanisms of Nucleation and Growth of Nanoparticles in Solution. *Chem. Rev.* **2014**, *114* (15), 7610−7630.
(33) Zhang, H.; Du, S.; Wang, Y.; Xue, F. Prevention of Crystal Agglomeration: Mechanisms, Factors, and Impact of Additives. *Crystals* **2024**, *14* (8), 676.
(34) van den Brand, D.; Mertens, V.; Massuger, L.; Brock, R. siRNA in ovarian cancer − Delivery strategies and targets for therapy. *J. Contr. Release* **2018**, *283*, 45−58.
(35) Liu, Y.; Yang, G.; Hui, Y.; Ranaweera, S.; Zhao, C.-X. Microfluidic Nanoparticles for Drug Delivery. *Small* **2022**, *18* (36), 2106580.
(36) Biswas, A. K.; Islam, M. R.; Choudhury, Z. S.; Mostafa, A.; Kadir, M. F. Nanotechnology based approaches in cancer therapeutics. *Adv. Nat. Sci.: Nanosci. Nanotechnol.* **2014**, *5* (4), No. 043001.
(37) Rodriguez-Loya, J.; Lerma, M.; Gardea-Torresdey, J. L. Dynamic Light Scattering and Its Application to Control Nanoparticle Aggregation in Colloidal Systems: A Review. *Micromachines* **2023**, *15* (1), 24.
(38) Fissan, H.; Ristig, S.; Kaminski, H.; Asbach, C.; Epple, M. Comparison of different characterization methods for nanoparticle dispersions before and after aerosolization. *Anal. Methods.* **2014**, *6* (18), 7324−7334.
(39) Hao, Z.; Li, C.; Yu, J.; Zhang, X.; Ran, F.; Dai, L.; Shen, Z.; Qiu, Z.; Wang, J. Lignin particles as green pore-forming agents for the fabrication of microporous polysulfone membranes. *Int. J. Biol. Macromol.* **2023**, *241*, No. 124603.
(40) Meléndrez, M. F.; Cárdenas, G.; Arbiol, J. Synthesis and characterization of gallium colloidal nanoparticles. *J. Colloid Interface Sci.* **2010**, *346* (2), 279−287.
(41) Zhang, W.; Mehta, A.; Tong, Z.; Esser, L.; Voelcker, N. H. Development of Polymeric Nanoparticles for Blood−Brain Barrier

Transfer—Strategies and Challenges. *Adv. Sci.* **2021**, *8* (10), No. 2003937.
(42) Ferro, C.; Florindo, H. F.; Santos, H. A. Selenium Nanoparticles for Biomedical Applications: From Development and Characterization to Therapeutics. *Adv. Healthcare Mater.* **2021**, *10* (16), No. 2100598.
(43) Gautam, M.; Kim, J. O.; Yong, C. S. Fabrication of aerosol-based nanoparticles and their applications in biomedical fields. *J. Pharm. Investig.* **2021**, *51* (4), 361−375.
(44) Buxton, G. A. The fate of a polymer nanoparticle subject to flow-induced shear stresses. *Europhys. Lett.* **2008**, *84* (2), 26006.
(45) Levit, S. L.; Walker, R. C.; Tang, C. Rapid, Single-Step Protein Encapsulation via Flash NanoPrecipitation. *Polymers* **2019**, *11* (9), 1406.
(46) Adelnia, H.; Blakey, I.; Little, P.; Ta, H. Poly(succinimide) Nanoparticles as Reservoirs for Spontaneous and Sustained Synthesis of Poly(aspartic acid) under Physiological Conditions: Potential for Vascular Calcification Therapy and Oral Drug Delivery. *J. Mater. Chem. B* **2023**, *11*, 2650−2662.

https://doi.org/10.1021/acsanm.5c04092
ACS Appl. Nano Mater. 2025, 8, 19658−19667